HIGH-ORDER LARGE EDDY SIMULATION AROUND 2-D AEROFOIL WITH HIGH-LIFT DEVICE

***Takahiro Sumi, *Takuji Kurotaki and *Jun Hiyama**
***Aerospace Research and Development Directorate, Japan Aerospace Exploration Agency**

Keywords: *LES, Multi-block, Interface Condition, High-lift Device*

Abstract

An advanced method of high-order multi-block computation with the generalized characteristic interface conditions (GCIC) is newly proposed and realized. The large eddy simulation (LES) with the GCIC is applied to solve a realistic flow problem around complex geometry such as a two-dimensional aerofoil with a high-lift device.

1 Introduction

Recently, high-order finite difference method (FDM) with structured grid [1] has been widely applied to detailed computations such as the large eddy simulations (LES) and the direct numerical simulations (DNS). In practical computation with an inadequate grid, numerical instability is frequently observed around singular points with metric discontinuity. Generally, it is hard to generate an ideal smooth single grid around complex geometry. Even in conventional multi-block computation using a method with overlapped domains, it is necessary to pay great attention to grid continuity on the block interface.

Kim et al. have originally developed the characteristic interface conditions (CIC) [2] and solved the above singular problem by block decomposition along the singular surface and by imposition of the CIC on the block interface. In this procedure, spatial differentiation is independently performed in each isolated block and does not cross the block interface, and which successfully results in producing no numerical oscillations. However, the original theory has constraints on the mathematical treatment of the block interface, and prevents numerical robustness and flexibleness resultantly from a practical point of view. Therefore, in order to extend the functions of the CIC, the authors have newly developed the generalized characteristic interface conditions (GCIC) [3] based on the similar concept of the original theory.

In the present study, in respect of practical application, the LES with the GCIC is performed to solve a realistic flow problem around complex geometry such as a 2-D aerofoil with a high-lift device. An advanced method of multi-block computation with the GCIC is newly proposed and realized, and its excellent performance is shown as a result.

2 Generalized Characteristic Interface Conditions

In this section, mathematical outline of the GCIC are briefly described. The upper side of Fig. 1 shows a two-dimensional structured grid with singular points as a single domain. In the points represented by black circles, the metrics at the left side limit and those at the right side limit have no correspondence each other. In order to avoid these singularities, as shown in the lower side of Fig. 1, the single domain is decomposed into two blocks along the singular line, and proper characteristic interface conditions are effectively imposed on the block interface.

The transformed non-conservative form of the 3-D Navier-Stokes equations in the generalized curvilinear coordinates can be expressed as

$$\frac{\partial \boldsymbol{U}}{\partial t} + \xi_x \frac{\partial \boldsymbol{E}}{\partial \xi} + \xi_y \frac{\partial \boldsymbol{F}}{\partial \xi} + \xi_z \frac{\partial \boldsymbol{G}}{\partial \xi} + \boldsymbol{D} = 0, \quad (1)$$

where $\boldsymbol{D}$ represents the summation term of the tangential convective flux derivatives and all viscous flux derivatives. Then, the following two kinds of matrices are introduced:

$$\boldsymbol{P} = \frac{\partial \boldsymbol{U}}{\partial \boldsymbol{V}},\ \boldsymbol{S} = \frac{\partial \boldsymbol{V}}{\partial \boldsymbol{W}}, \tag{2}$$

where the matrix $\boldsymbol{P}$ is the Jacobian matrix between the conservative variables and the primitive variables, and the matrix $\boldsymbol{S}$ is that between the primitive variables and the characteristic variables, respectively. By using these terms, Eq. (1) can be rewritten as the following characteristic equations:

$$\frac{\partial \boldsymbol{U}}{\partial t} + \boldsymbol{PSL} + \boldsymbol{D} = 0, \tag{3}$$

where $\boldsymbol{L}$ represents the characteristic wave amplitude variation vector given by

$$\boldsymbol{L} = \boldsymbol{S}^{-1}\boldsymbol{P}^{-1}\left(\xi_x \frac{\partial \boldsymbol{E}}{\partial \xi} + \xi_y \frac{\partial \boldsymbol{F}}{\partial \xi} + \xi_z \frac{\partial \boldsymbol{G}}{\partial \xi}\right). \tag{4}$$

The GCIC are started from the intuitive fact that the time derivatives of the conservative variables at the left side limit and those at the right side limit on the block interface are strictly matched. From Eq. (3), these conditions are replaced by the spatial relations and are simply expressed as follows:

$$\left(\frac{\partial \boldsymbol{U}}{\partial t}\right)^l = \left(\frac{\partial \boldsymbol{U}}{\partial t}\right)^r \Leftrightarrow \boldsymbol{P}^l\boldsymbol{S}^l\boldsymbol{L}^l + \boldsymbol{D}^l = \boldsymbol{P}^r\boldsymbol{S}^r\boldsymbol{L}^r + \boldsymbol{D}^r, \tag{5}$$

and which can be arranged into following two kind forms,

$$\begin{aligned} \boldsymbol{L}^l &= \left(\boldsymbol{S}^l\right)^{-1}\left[\boldsymbol{S}^r\boldsymbol{L}^r + \left(\boldsymbol{P}^l\right)^{-1}\left(\boldsymbol{D}^r - \boldsymbol{D}^l\right)\right], \\ \boldsymbol{L}^r &= \left(\boldsymbol{S}^r\right)^{-1}\left[\boldsymbol{S}^l\boldsymbol{L}^l + \left(\boldsymbol{P}^r\right)^{-1}\left(\boldsymbol{D}^l - \boldsymbol{D}^r\right)\right]. \end{aligned} \tag{6}$$

Based on the sign of the contravariant velocity perpendicular to the block interface, $\boldsymbol{L}$ is directly computed from Eq. (4) in case it is positive, but is corrected by using Eq. (6) in case it is negative. As a result, the modified convective flux derivatives are expressed as follows,

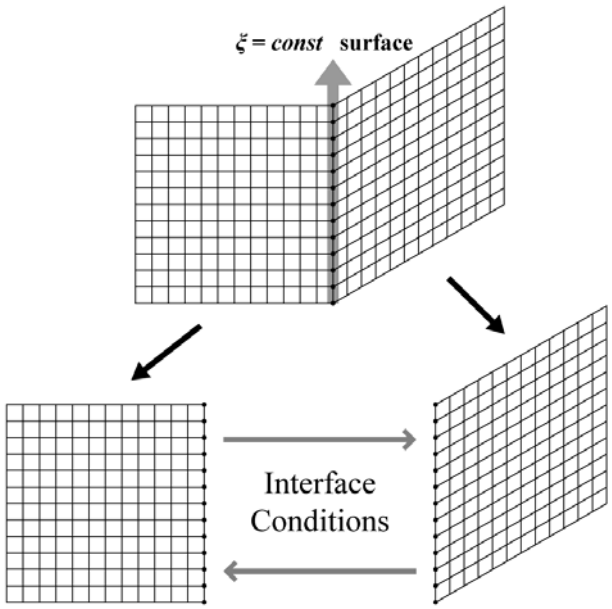

Fig. 1. Concept of Multi-block Computation using Characteristic Interface Conditions.

$$\xi_x \frac{\partial \boldsymbol{E}}{\partial \xi} + \xi_y \frac{\partial \boldsymbol{F}}{\partial \xi} + \xi_z \frac{\partial \boldsymbol{G}}{\partial \xi} = \boldsymbol{PSL}^*. \tag{7}$$

At last, the time integration can be performed in the same manner as the inner computational points:

$$\left(\frac{\partial \boldsymbol{U}}{\partial t}\right)^* = -\boldsymbol{PSL}^* - \boldsymbol{D}. \tag{8}$$

More detailed formulation can be seen in Ref. [3].

3 LES on NLR7301 Two-element Aerofoil

In the following section, an numerical example of LES on the NLR7301 two-element aerofoil is shown and discussed, which was one of the workshop subjects of the European computational aerodynamics research project (ECARP) in 1990s [4] and was experimentally investigated in the National Aerospace Laboratory (NLR) of Netherlands. [5]

3.1 Numerical Procedures

The 3-D Navier-Stokes equations are used as the governing equations. The spatial derivatives of the convective and viscous flux terms are

Table 1. Summary of Numerical Conditions.

	Case 1	Case 2
Angle of attack (deg)	13.1	6.0
Flap deflection angle (deg)	20.0	
Gap width (%)	2.6	1.3
Overlap width (%)	5.3	
Reynolds number	$2.51*10^6$	
Mach number	0.185	
Number of zones	39	47
Number of points (Span wise)	6,891,534 (26)	10,105,752 (31)

solved by the optimized 6th order tri-diagonal (OSOT) compact difference scheme suggested by Kim et al. [6] (On the boundary and the near points of the boundary, the order of accuracy is gradually decreased from 6 to 2 for numerical stability. [7] This scheme maintains tri-diagonal Padé form, and has the maximum spatial resolution, optimizing dissipation and dispersion errors simultaneously. For the time integration, the low storage type of 2 step 4th order low dissipation and low dispersion Runge-Kutta (LDDRK) scheme proposed by Stanescu et al. [8] is used. This scheme increases numerical stability in the explicit time integration, and reduces dissipation and dispersion errors simultaneously. For the inflow and outflow boundary conditions, the Navier-Stokes characteristic boundary conditions (NSCBC) extended to the generalized curvilinear coordinates derived by Kim et al. [9, 10] are applied. In addition, in order to solve complex flow involving turbulence and transition, the advanced LES approach with the approximate deconvolution model (ADM) originally developed by Stolz et al. [11] is employed. In this method, an approximation of the unfiltered solution is obtained from the filtered solution by series expansion of a deconvolution operator. The effect of the sub-filtered scales is modeled by a relaxation regularization including a dynamically estimated relaxation parameter. Therefore, there is no need to explicitly compute the sub-grid scale closures and construct extra models for compressible flow.

3.2 Computational Model Descriptions

The flow conditions and the model configuration are set in take-off situation. Different two cases are investigated, and their numerical conditions are summarized in Table 1. The angles of attacks are chosen as 13.1 and 6.0 degrees, and the former is around one degree before stall. The flap was cut out from the main wing, and the aft part of the main wing was modified to get a smooth lower surface without flow separations. In order to realize a fully attached flow, the flap deflection angle is arranged at 20.0 degrees with a moderate value. The gap width between the main wing and the flap are chosen as 2.6 % and 1.3 % of the basic chord length of the main wing of 0.57 m in the experiment. The overlap width between the main wing and the flap are set to be 5.3 % of the basic chord length. The free stream Mach number and the Reynolds number are set to be 0.185 and $2.51*10^6$, respectively.

In the present study, block configurations and total grid numbers are investigated and changed in the two cases. Figure 2 shows typical decomposed multi-block configuration and grid for the computation, which are the enlargements of 20*20*0.1 computational domain. Total 39 and 47 zones are created and arranged around the two-element aerofoil, and the number of grid points is about 6.9 millions (26 equidistant points in the spanwise direction) and 10.1 millions (31 equidistant points in the spanwise direction) in total, respectively. Actually, the trailing edges of

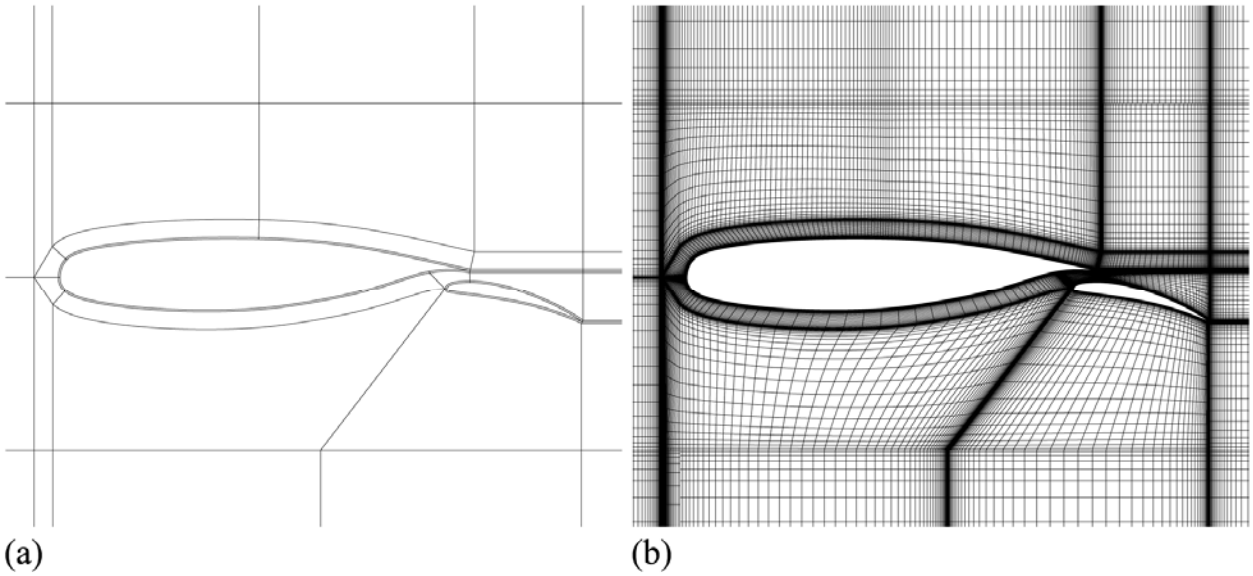

Fig. 2. (a) Decomposed Multi-block Configuration,
(b) Computational Grid (coarsened by a factor of 4 for visualization).

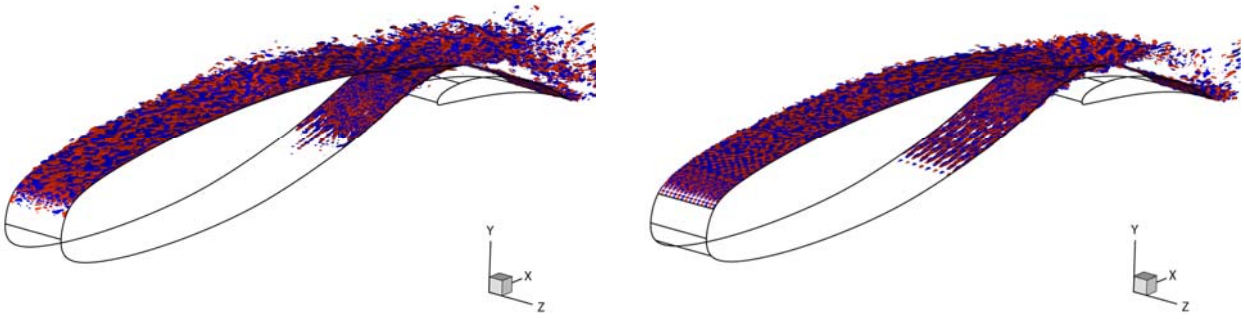

Fig. 3. Instantaneous Streamwise Vorticity Contours around NLR7301 Two-element Aerofoil,
Case 1 (left) and Case 2 (right).

the main wing and the flap used in the wind tunnel test are abruptly cut off with finite width. However, in the present computation, they are modified and sharpened like cusp shape for simplicity. The grid kinks on the block interface are positively employed everywhere by the application of the GCIC. Thereby, orthogonality of the grid is highly enhanced in each block, and mapping errors tend to decrease as a result. Besides, time cost of grid generation can be relatively low. The grid lines are clustered near the block interface in order to compensate accuracy drop of the finite difference scheme and improve the spatial resolution. In the spanwise direction, periodic conditions are imposed. On the other four block interface surfaces in each block, the signs of the contravariant velocity perpendicular to the block interface are calculated locally, and the GCIC are employed in every time step. The difficulty of the GCIC arises at multiple points appearing everywhere, where edges or corners of two or more blocks overlap and one-dimensional formulation of the GCIC cannot be applied exactly. Generally, at the multiple points, some round-off errors are accumulated with the time

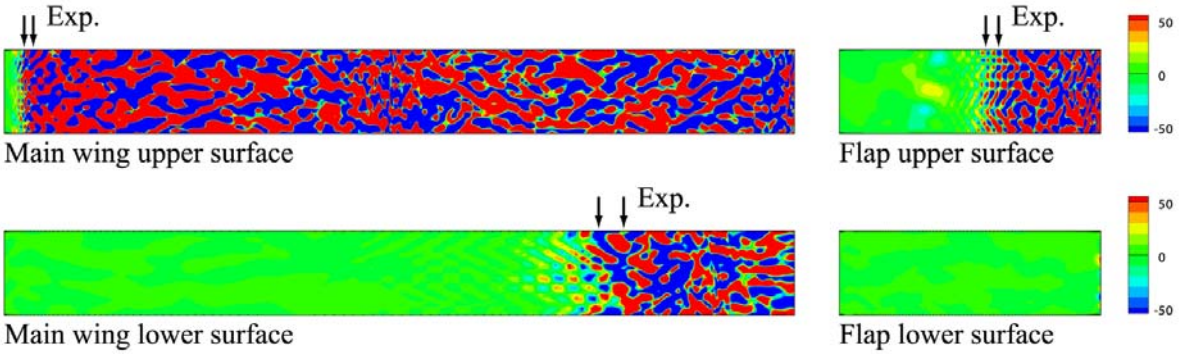

Fig. 4. Top Views of Instantaneous Streamwise Vorticity Contours near Aerofoil Surface in Case 1.

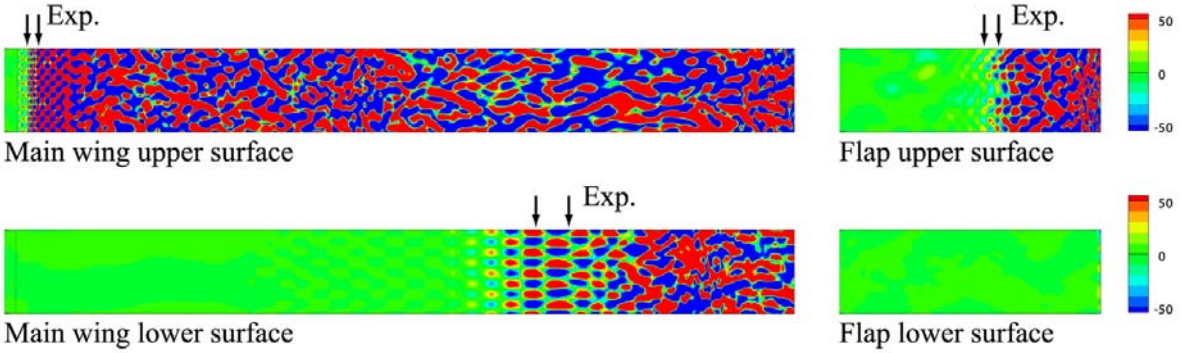

Fig. 5. Top Views of Instantaneous Streamwise Vorticity Contours near Aerofoil Surface in Case 2.

advancement of the computation even if all the points have the same initial state. However, this problem is satisfactorily solved by the iterative arithmetical averaging procedure of the primitive variables.

3.3 Results and Discussion

Figure 3 shows instantaneous streamwise vorticity contours in the vicinity of the aerofoil walls. The red and blue ones indicate different signs but the same absolute values. These are smoothly connected on the block interfaces, and no discontinuities can be observed anywhere. It is confirmed that the GCIC is well functioning and is successfully incorporated in the present LES. Several unsteady flow characteristics can be observed. On the upper surface of the main wing, transition from laminar to turbulent boundary layer flow can be observed with a small separation bubble. On the other hand, on the lower surface of the main wing and the upper surface of the flap, natural transition from laminar to turbulent boundary layer flow occurs much more downstream without laminar separation. Comparing the case 1 with the case 2, the flow of the former case with high angle of attack can be seen much more complicated rather than that of the latter case with low angle of attack.

In order to discuss the flow transition from laminar to turbulent boundary layer, several top views of the instantaneous streamwise vorticity contours near the aerofoil surface are shown in Fig. 4 and 5. The upper and lower surfaces of the main wing and the flap are separately drawn respectively, where arrows indicate the regions of the laminar separation bubble and the natural transition observed in the experiment. On the upper surface of the main wing, the laminar separation bubble plays an important role of the abrupt flow transition. The location of the laminar separation bubble in the case 1 is observed somewhat upstream rather than that in case 2. Furthermore, on the lower surface of the main wing and upper surface of the flap, the natural transition occurs accompanying the oblique wave. After the transition region, regularity of the flow is completely lost and

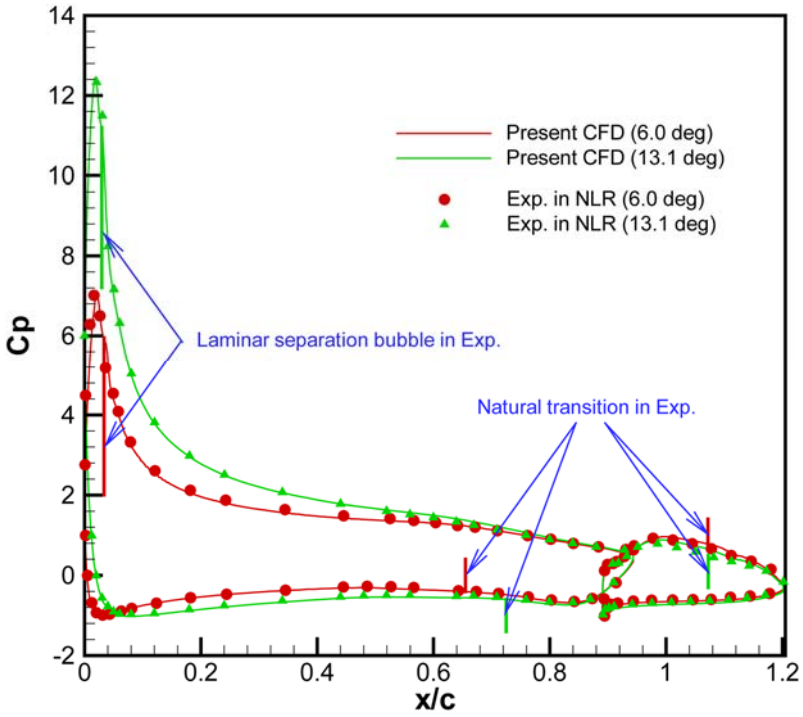

Fig. 6. Mean Pressure Coefficient along Chord Distance.

turbulent boundary layer is fully created. The natural transition on the lower surface of the main wing occurs more downstream in the case 1 compared with the case 2. On the upper surface of the flap, the locations of the natural transition are almost the same in the both cases. On the other hand, no transition phenomena can be observed on the lower side of the flap. Thus, on the transition regions around the aerofoil with high-lift device, qualitative agreements are obtained between the computation and the experiment. In spite of giving no information about the transition locations, the present LES can automatically capture and reproduce these transition phenomena around the complex geometry. This desirable capability is supposed to be mainly brought by the effective features of the ADM with sub-grid scale characteristics. The detailed discussions on the flow natural transition around the NACA0012 based on the same numerical procedure are found in the companion paper. [12, 13]

Figure 6 shows mean pressure coefficient along non-dimensional chord distance. The solid lines and the symbols indicate the present computational results and the experimental results, respectively. In the figure, the locations of the laminar separation bubble and the natural transition observed in the experiment are also written together. A relatively high suction peak is seen to occur on the upper surface of the main wing nose. Shortly downstream of the suction peak, a small inflection point is observed where transition from laminar to turbulent boundary layer flow occurs by the small separation bubble. The computational results have quantitative agreements with the experimental results on the main wing surface in the both cases. However, the computation slightly overestimates the distributions on the upper surface of the flap. This main reason is supposed to be mainly brought by the modification of the trailing edge shape of the main wing in the present computation.

Figure 7 shows boundary layer velocity profiles in the case 1. In the experiment, the hot-wire technique was employed and was traversed along perpendicular direction on the aerofoil surface defined in the figure. Distributions at different five locations are available. [4] As described above, in the Station 8, large difference can be seen compared with the experiment due to mainly the modification of the trailing edge shape of the main wing. As a result, from the Station 12 to Station 16 of the upper side and the wake of the flap, velocity

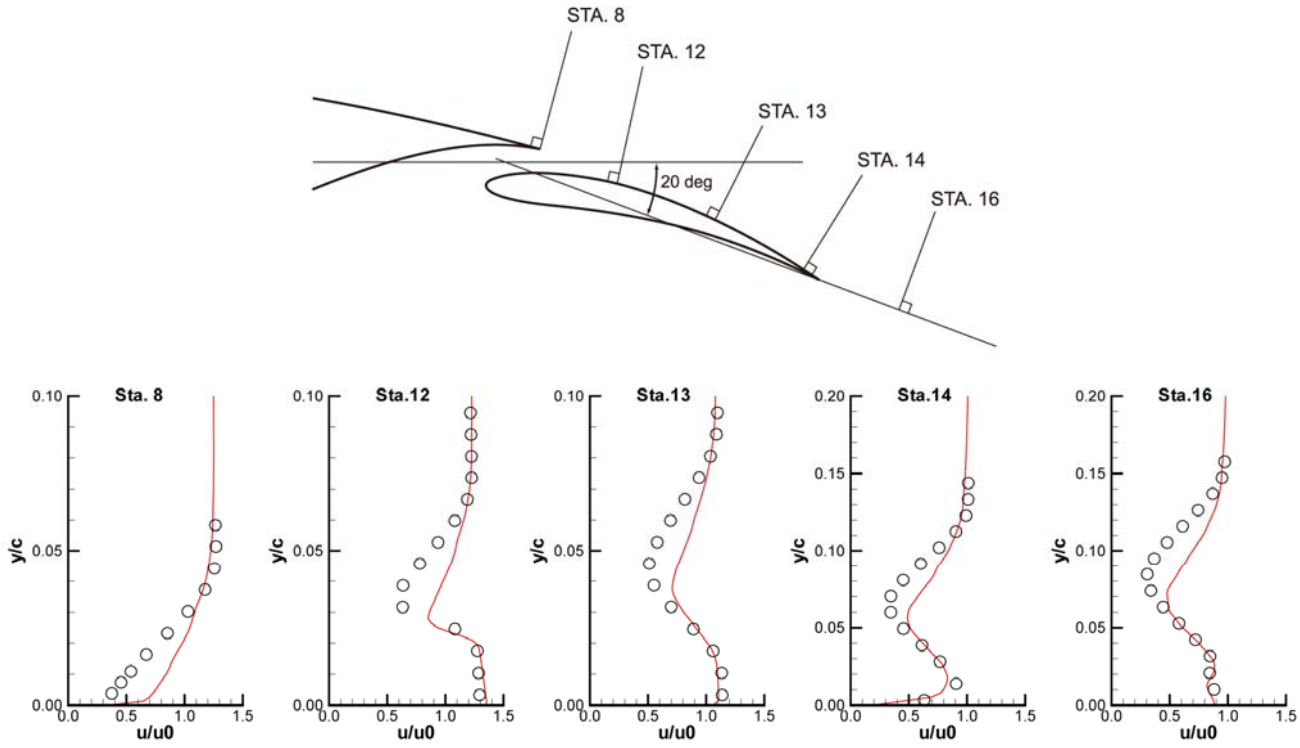

Fig. 7. Boundary Layer Velocity Profiles in Case 1.

distributions on the boundary layer are strongly influenced by the wake of the main wing, and velocity deficit is slightly underestimated in the computation. However, qualitative agreements are obtained between the computational results and the experimental results.

4. Conclusions

A new concept of high-order multi-block computation with the GCIC is proposed and realized, and its performance is shown and discussed. By applying the GCIC in the multi-block computation, abrupt grid kinks on the block interface can be intentionally employed, and decomposed block with simple geometrical topology can be easily arranged around the complex geometry. Consequently, grid orthogonality is highly enhanced in each block, and mapping error tends to decrease. This is preferable feature for the high-order fluid computation using the FDM with structured grid.

As a preliminary study, the LES with the GCIC is applied to the flow simulation around the NLR7301 two-element aerofoil. It is confirmed that the GCIC is well functioning and is successfully incorporated in the computation. The present LES can automatically capture and reproduce transition phenomena around the complex geometry without a priori information about the flow transition locations. On the mean pressure coefficients and the velocity profiles, qualitative agreement is obtained compared with the experimental results. However, some subjects still remain for quantitative prediction. As the further study, trailing edge shape of the aerofoil, grid resolution, sub-grid scale model in the LES etc. have to be comprehensively checked and investigated in order to improve the performance of the present computational technique.

References

[1] Lele S., Compact Finite Difference Schemes with Spectral-like Resolution, *Journal of Computational Physics*, Vol. 103, pp. 16-42, 1992.

[2] Kim J. and Lee D., Characteristic Interface Conditions for Multiblock High-order Computation on Singular Structured Grid, *AIAA Journal*, Vol. 41, pp. 2341-2348, 2003.

[3] Sumi T., Kurotaki T. and Hiyama J., Generalized Characteristic Interface Conditions for High-order

Multi-block Computation, *International Journal of Computational Fluid Dynamics*, Vol. 21, pp. 335-350, 2007.
[4] Arlinger B. and Larsson T., NLR 7301 Two-element Airfoil at High Lift, *Notes on Numerical Fluid Mechanics*, Vol. 58, pp. 375-396, 1997.
[5] Van den Berg B. and Oskam B., Boundary Layer Measurements on a Two-dimensional Wing with Flap and Comparison with Calculations, *NLR TR* 79009 U, 1979.
[6] Kim J. and Lee D., Optimized Compact Finite Difference Schemes with Maximum Resolution, *AIAA Journal*, Vol. 34, pp. 887-893, 1996.
[7] Kim J. and Lee D., Implementation of Boundary Conditions for Optimized High-order Compact Schemes, *Journal of Computational Acoustics*, Vol. 5, pp. 177-191, 1997.
[8] Stanescu D. and Habashi W., 2N-storage Low Dissipation and Dispersion Runge-Kutta Schemes for Computational Acoustics, *Journal of Computational Physics*, Vol. 143, pp. 674-681, 1998.
[9] Kim J. and Lee D., Generalized Characteristic Boundary Conditions for Computational Aeroacoustics, *AIAA Journal*, Vol. 38, pp. 2040-2049, 2000.
[10] Kim J. and Lee D., Generalized Characteristic Boundary Conditions for Computational Aeroacoustics, Part 2, *AIAA Journal*, Vol. 42, pp. 47-55, 2004.
[11] Stolz S., Adams N. and Kleiser L., The Approximate Deconvolution Model for Large Eddy Simulations of Compressible Flows and Its Application to Shock-turbulent-boundary-layer Interaction, *Physics of Fluids*, Vol.13, pp. 2985-3001, 2001.
[12] Kurotaki T., Sumi T., Atobe T. and Hiyama J., Numerical Simulation around Aerofoil with High Resolution in High Reynolds Numbers, *AIAA paper* 2007-720, 2007.
[13] Kurotaki T., Sumi T., Atobe T. and Hiyama J., Numerical Simulation around Airfoil with Natural Transition in High Reynolds Numbers, *AIAA paper* 2007-3841, 2007.

Copyright Statement